Superconducting resistive transition in coupled arrays of 4 Å carbon nanotubes

Zhe Wang, Wu Shi, Hang Xie, Ting Zhang, Ning Wang, Zikang Tang, Xixiang Zhang,[*] Rolf Lortz, and Ping Sheng[†]
Department of Physics and William Mong Institute of Nano Science and Technology, HKUST, Clear Water Bay, Kowloon,
Hong Kong, China

Ilya Sheikin and Albin Demuer
Grenoble High Magnetic Field Laboratory, CNRS, 25 Avenue des Martyrs, BP 166, 38042 Grenoble, France

We report superconducting resistive transition characteristics for array(s) of coupled 4 Å single wall carbon nanotubes embedded in aluminophosphate-five zeolite. The transition was observed to initiate at 15 K with a slow resistance decrease switching to a sharp, order of magnitude drop at $\sim$7.5 K. The latter exhibits anisotropic magnetic field dependence, and the differential resistance versus current (voltage) measurements show a rich variety of details that are consistent with the establishment of coherence, in stages, as the temperature is lowered below 15 K. In particular, the resistance drop that starts at 7.5 K exhibits attributes that are consistent with the manifestations of a Berezinskii-Kosterlitz-Thouless transition that establishes quasi-long-range order in the plane transverse to the c axis of the aligned nanotubes.

I. INTRODUCTION

Superconductivity in carbon nanotubes has been controversial because carbon is not known to be a superconducting element, and if there is indeed superconducting tendency in carbon nanotubes[1] (the large curvature of small carbon nanotubes can potentially open electron-phonon couplings that are absent in the graphene sheet, thereby enhancing the prospect for superconductivity), its manifestation could be quenched by long wavelength thermal fluctuations[2] as well as by the Peierls distortion that favors an insulating ground state.[3] In this context the earlier report on the Meissner effect in 4 Å carbon nanotube-zeolite composites[4] and the more recent observation of their superconducting specific heat signals[5] have only deepened the mystery on the specific manner, in which the nanotube superconductivity comes into being, and on whether there can be a sharp superconducting resistive transition that is usually taken to be the hallmark of a superconductor.

In this work, we show that by devising strategy to make surface electrical contacts to the samples that are separated by only 100 nm, reliable and repeatable observations of the superconducting resistive transition can be obtained. The measured results show a resistive transition that initiates at 15 K switching to a sharp drop at around 7.5 K, with an attendant richness of details that serve as the basis for physical interpretation. In particular, the temperature dependence of the resistance and its associated nonlinear I-V characteristics are consistent with the physical picture of a coupled Josephson array, comprising aligned nanotubes, crossing over from an individually fluctuating one-dimensional (1D) system to a coherent three-dimensional (3D) superconductor—mediated by a Berezinkii-Kosterlitz-Thouless (BKT) transition,[6,7] which establishes quasi long range order in the transverse ab plane perpendicular to the c axis of the nanotubes. The attainment of overall coherence across the measuring electrodes (denoted as global coherence in this work) is seen at even lower temperatures.

In what follows, description of sample preparation, sample geometry, and measurement details in Sec. II are fol-

lowed by the presentation of experimental data in Sec. III that comprise the temperature dependence of resistance $R(T)$, magnetoresistance and its anisotropy, plus differential resistance dV/dI measured as a function of the current I. In Sec. IV, we present our interpretation of the data by considering the transverse coupling of the nanotubes in the ab plane as the basis for the sharp resistive transition. It is shown that both the nonlinear I-V characteristics and the $R(T)$ behaviors are consistent with the manifestations of a BKT transition in the ab plane that coherently couples the nanotubes, thereby accomplishing the 1D to 3D crossover. We conclude in Sec. V by noting some of the still unexplained phenomena and the works to be done.

II. SAMPLE PREPARATION AND MEASUREMENT GEOMETRY

The 4 Å carbon nanotubes are embedded in the pores of AFI zeolite crystals that are generally 100 μm wide and 500 μm in length. The straight pores of the AFI zeolite are aligned along the c axis with a center-to-center separation of 1.37 nm. They form a two-dimensional (2D) close-packed lattice in the ab plane transverse to the c axis. The inner diameter of the pores, after discounting the size of the oxygen atoms lining the walls, is 0.7 nm.[8] The embedded nanotubes were prepared by first heating the crystal in 0.3 atm of oxygen and 0.7 atm of N_2 or Ar at 580 °C for 4 h. The purpose of this initial heating stage is to remove the precursor—tripropylamine—that was present in the pores of the as-grown crystals. At the end of the first heating stage the crystals were transparent with no Raman signals for carbon-carbon bonds. Subsequently the 0.3 atm of O_2 was replaced by ethylene and the crystal was heated at the same temperature for the same duration. The resulting crystals show strong optical polarization anisotropy with Raman radial breathing modes at both 510 cm^{-1} [for the (4,2) chirality] and 550 cm^{-1} [for the (5,0) chirality]. In particular, the peak at the 550 cm^{-1} is about 10% the height of the G band at
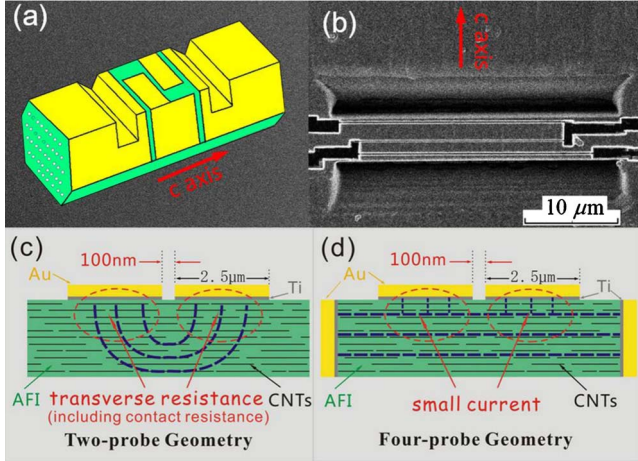
FIG. 1. (Color online) (a) Cartoon picture of the sample. Yellow denotes gold and green denotes AFI crystal surface exposed by FIB etching. Nanotubes are delineated schematically by open circles. (b) SEM image of the sample. The *c* axis is along the N-S direction. The thin, light, horizontal line in the middle is the 100 nm separation between the two surface voltage electrodes that are on its two sides. The dark regions are the grooves cut by the FIB and sputtered with Au/Ti to serve as the end-contact current electrodes. (c) and (d) show schematic drawings of the two-probe and four-probe geometries, respectively. Blue dash lines represent the current paths. In (d), the two end-contact current pads are 4 μm in depth and 30 μm in width.

1600 cm^{-1} for the C-C bonds.[5] We attribute the superconducting behavior to the (5,0) nanotubes.

It should be noted that the 4 Å carbon nanotubes have been previously characterized by direct transmission electron microscope observation (after dissolving the AFI matrix),[9] polarized and resonant Raman scattering,[10,11] plus comparisons between first principle calculations and absorption spectra.[12,13]

Figure 1 shows both a cartoon picture [Fig. 1(a)] of the AFI zeolite crystal with the four-probe contact geometry, as well as a scanning electron microscope (SEM) image of an actual sample [Fig. 1(b)]. Here the crystal was prepared by first cutting two troughs in an AFI crystal (50×50 ×500 μm) with focused ion beam (FIB, Seiko SMI2050). The troughs, 4 μm in depth and 30 μm in width, are separated by a 5 μm slice that is perpendicular to the *c* axis [Fig. 1(a)].

The AFI crystal (with embedded carbon nanotubes), thus prepared, was sputtered with 50 nm of Ti and 150 nm of Au. The electrical contact geometry was subsequently delineated by using the FIB to remove the Au/Ti film in a predesigned pattern, shown in Fig. 1(a). The FIB delineated areas are clearly visible in the SEM image shown in Fig. 1(b). Here, the outer electrodes make end contacts to the nanotubes, whereas the two inner electrodes, each about 2.5 μm wide, are separated by 100 nm and are on the surface of the AFI crystal. As the nanotubes are only ~1 nm below the surface, which is imperfect in any case, the surface contact electrodes enables the measurement of electrical characteristics transverse to the *c* axis of the nanotubes. We have carried out measurements using both the four-probe (with the outer con-

tacts as the current electrodes) and two-probe geometry. In Figs. 1(c) and 1(d) we show schematically the two-probe and four-probe measurement geometries. In the former the two surface-contact electrodes were used. In what follows we show results mostly done in the two-probe geometry. Use of the four-probe geometry is noted whenever such result is presented, as *the difference between the four-probe and the two-probe results is essentially the transverse resistance* [Figs. 1(c) and 1(d)]. In addition, the observation of the resistive transition in both the two-probe and the four-probe geometries tends to exclude the electrical contacts as the source of the exhibited behavior.

The transport measurements were carried out in the Quantum Design Physical Property Measurement System, with a 2.1 Ω series resistance. Both resistance and differential resistance were measured using Keithley 2182A nanovoltmeter and 6221 AC/DC source.

It should be mentioned that the measured resistances by using the two current electrodes (with end contacts) were always very large, on the order of hundreds of kilohms. No sharp resistive transition was observed in that configuration. However, we did observe magnetoresistance below 10–15 K in such a configuration for some samples, which may be interpreted as a weak sign for superconductivity. We have also tried to measure the transverse resistance directly by placing the electrodes across the two opposite facets of the AFI crystal. The measured resistances were even larger, on the order of tens of megaohms with a temperature dependence that increased too fast at low temperatures for detecting any reliable signs of a resistive transition or magnetoresistance. These results stress the importance of having the measuring electrodes close together so as to achieve small resistance.

III. EXPERIMENTAL RESULTS

In this section, we present the measured results on two samples that were fabricated identically. However in sample 2 one of the current electrodes (with end contacts to the nanotubes) was unintentionally (electrically) shorted with the closest voltage (surface contact) electrode. Hence only the three-probe (the shorted electrode acting as both the current and voltage electrode) and two-probe measurements were possible for sample 2.

A. Temperature dependence of resistance

Figures 2(a) and 2(b) show the measured resistance plotted as a function of temperature for samples 1 and 2, respectively. Both show a sharp drop starting at ~7.5 K, which moves to lower temperatures with applied magnetic field (perpendicular to the *c* axis in this case). That the transition is sensitive to the magnetic field means that the superconducting behavior must originate from an array of coupled nanotubes at least a few tens of nanometers in its transverse size.[14] In the inset to Fig. 2(a) we show an enlarged upper section of the curves from 3 to 20 K. For $T > 17$ K the curves are very good straight lines with a slight negative slope; the data shown in the inset are relative to this straight-
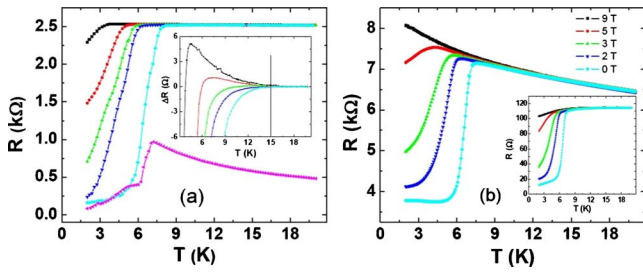
FIG. 2. (Color online) Temperature dependence of resistance: (a) for sample 1 and (b) sample 2. Both measured with 1 μA current. The same color of the line represents the same magnetic filed in (a), (b) and insets. (a) The magenta curve is the four-probe data at zero field and the others are two-probe data. Inset: A magnified view of the upper section from 3 to 20 K with the straight-line asymptote above 17 K subtracted. The superconducting transition clearly begins at 15 K. (b) Two-probe data of sample 2 show similar sharp resistance drop as sample 1. Inset shows the three-probe data that display a much smaller resistance.

line asymptote, extended to lower temperatures. They clearly show the initiation of the whole transition process starts at 15 K. While the resistance changes are small, their magnetic field dependence is unmistakable. The four-probe result, measured at zero field, is also displayed for comparison with the two-probe case. It is seen that the difference between the two-probe and four-probe results nearly disappeared below 5 K, indicating a clear change in the transverse resistance. The four-probe data also show that there could be two stages in reaching global coherence, since after the sharp drop there is still a gradual further decrease in the resistance. Coupled with the fact that above 7.5 K the four-probe data display a nonmetallic temperature behavior, a consistent explanation is that there are weak links along the c axis which turned superconducting at temperatures below 5 K. This point is reinforced by the I-V characteristics as shown below. For sample 2, Fig. 2(b) shows a similar behavior, although the resistance values are much larger. Here, the three-probe result, shown in the inset, is seen to give an order of magnitude smaller resistance values. Together with the information provided by the differential resistance measurements [Fig. 7(a), the 2 K curve], it is concluded that there is a ~4 kΩ contact resistance (between the electrodes and the sample surface) in sample 2 that is external to the system of coupled nanotubes.

B. Magnetoresistance

In Figs. 3(a) and 3(b), we show the magnetoresistance (MR) for samples 1 and 2 at different temperatures. Here the magnetic field was applied perpendicular to the c axis. At 2 K, there is a clear transition point at 2–3 T. For comparison, four-probe data are also shown for sample 1. It is instructive that the measured resistances for the two sets of data are almost identical below 2 T but diverge above that. This phenomenon implies that at a magnetic field of 2 T or larger the resistance in the transverse ab plane is markedly increased, i.e., a change in the resistive state has occurred. Figure 3(c) shows the observed anisotropy in magnetoresistance for sample 2, measured at 5 T in the two-probe geometry. The
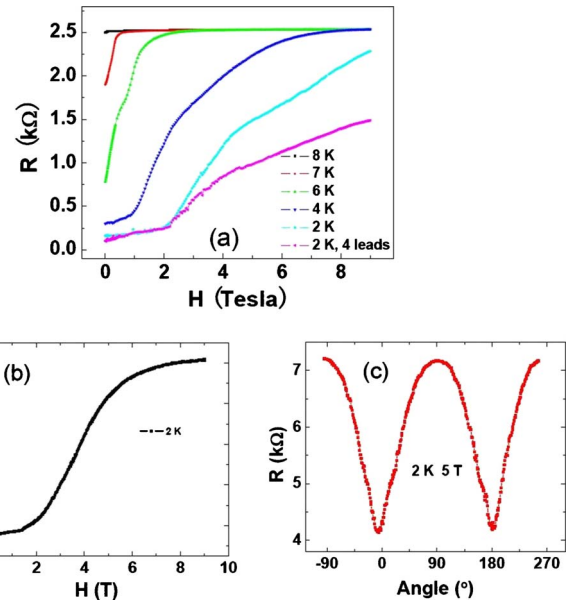

FIG. 3. (Color online) (a) MR of sample 1 under different temperatures, the magenta curve being the four-probe data. The measurement current is 1 μA. (b) MR of sample 2 at 2 K. (c) MR anisotropy of sample 2 measured with two probe geometry. The angle is between the magnetic field and the c axis.

anisotropy tells us that a magnetic field perpendicular to the c axis is more effective in suppressing the superconducting behavior than the same field applied parallel to the c axis. This is reasonable since the magnetic susceptibility should be larger for the perpendicular field, owing to the larger conductivity along the c axis as compared to the transverse conductivity.

1. MR oscillations at small measuring currents

An interesting phenomenon—oscillation in the magnetoresistance as a function of applied magnetic field—was observed at low measurement currents. In Fig. 4(a) we show the MR data measured with a small current, i.e., 100–300 nA at 2 K, to exhibit many reproducible oscillations that may be interpreted as arising from the Aharonov-Bohm effect associated with supercurrent loops penetrated by a magnetic flux,
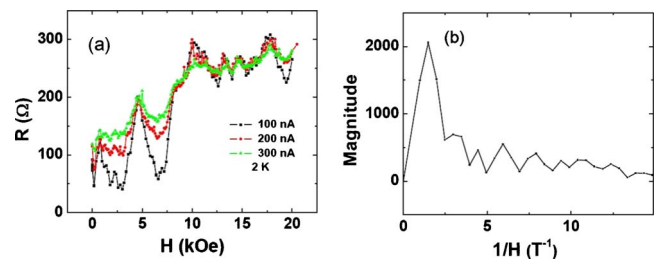

FIG. 4. (Color online) MR of sample 1 measured at 2 K with small currents. Reproducible oscillations are clearly seen. They disappear at large current levels or at higher temperatures. (b) Fourier transformation of (a), which shows the periods of the oscillations to range from 1680 to 6700 Oe with the dominant period being 6700 Oe.
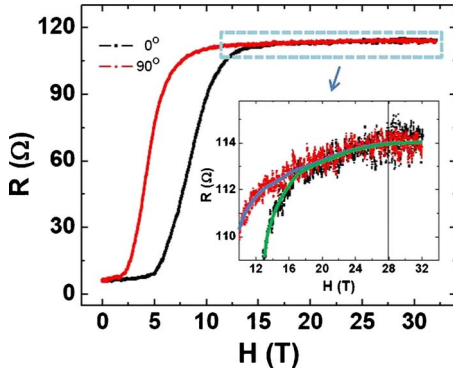
FIG. 5. (Color online) MR of sample 2 with magnetic field parallel (0°) or perpendicular (90°) to the *c* axis, measured with the three-probe configuration at 50 mK. Inset: A magnified view of the upper section. Clearly the two curves merge at around 18 Tesla, and the merged curve maintains a positive slope up to 28 Tesla, beyond which the MR is nearly constant. A slight kink at 28 T is discernible.

in which constructive or destructive interference can increase or decrease the amount of supercurrent that passes through the loop. When these loops are embedded in the overall sample network, the interference effect is manifest as an increase or decrease in MR. By Fourier transforming the data, shown in Fig. 4(b), one can identify the periods of the oscillations to range from 1680–6700 Oe, with the 6700 Oe being the dominant period. That may be translated into current loops that are ∼56–110 nm in size (by assuming a periodicity of $\phi_o = hc/2e$). At larger current levels or higher temperatures, the higher phase slip rate (and the associated higher resistances in accordance with the Josephson rule) tends to wash out the effect.

2. High-field measurements

We have measured MR up to 32 T, at 50 mK, at the Grenoble High Magnetic Field Laboratory. Shown in Fig. 5 are the results for sample 2 (with the three-probe geometry) under both the perpendicular and parallel magnetic fields. There are two notable features. The first is the magnetic anisotropy as evidenced by the clear lateral separation of the two curves. The second is the characteristic S shape of the curve, with the first turning point at 2 and 5 T for the perpendicular and parallel fields, respectively, and the second turning point at 10 and 13.5 T. The two curves merge at ∼18 T but the magnetoresistance continues to increase moderately up to 28 T. This is seen in the inset to Fig. 5. In the following section, we interpret the two turning points to be the demarcations between the different degrees/stages of coherence in the system. We also speculate on a potentially interesting scenario for the "superconducting state" in the range of 18–28 T.

C. Differential *I-V* characteristics

In Figs. 6 and 7, we show measured differential resistance plotted as a function of the current for samples 1 and 2, respectively. Both were measured under the two-probe ge-
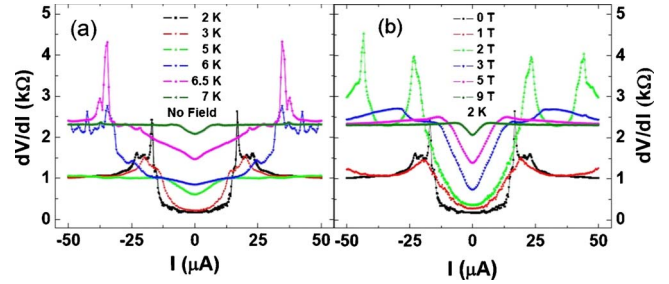

FIG. 6. (Color online) Current dependence of the differential resistance for sample 1. (a) The supercurrent gap (i.e., the low resistance region) of 2 K disappears in stages when temperature increases. Above 6 K, transverse coherence deteriorates, and the shape of the quasigap is a reflection of the BKT transition's nonlinear *I-V* behavior at $T < T_{co}$. (b) Increasing magnetic field has a similar effect as increasing the temperature. The coherent oscillations that appear at 2 T remain unexplained.

ometry. Here, the two samples display some differences that will be discussed below.

For sample 1, Fig. 6(a), the most striking feature is the existence of two (large-current) resistance plateaus, one at 1 kΩ and the other at 2.3 kΩ. The latter is associated with the transition at 7.5 K. In the presence of large series resistance, differential resistance measurement can help to reveal the intrinsic *I-V* characteristics associated with the 7.5 K transition. As the temperature is lowered below 7.5 K, it is seen from Fig. 6(a) that a triangular quasigap develops which eventually merges into the 2.3 kΩ plateau. As the temperature is lowered to 6 K, the quasigap is seen to become more rounded. A linear variation of the differential resistance *R* vs current *I* implies $V \propto I^2$, and the progressive variation from a constant *R* ($V \propto I$) to a more rounded gap (as the temperature is lowered) is consistent with the behavior of $V \propto I^\alpha$, where α varies from 1 to 3 or larger with decreasing temperature. A particularly instructive curve is the one at 6 K (blue), which shows that the bottom of the quasigap coincides with the 1 kΩ plateau. This is consistent with the physical picture that the 1 kΩ resistance originates from the weak links along the *c*-axis direction. Thus in order to analyze the nature of the 7.5 K transition, this 1 kΩ series resistance ought to be subtracted.

At around 5 K, a smaller gap is seen to develop which is associated with the 1 kΩ plateau. At low temperatures a low resistance region/gap becomes well-defined. The sharp co-
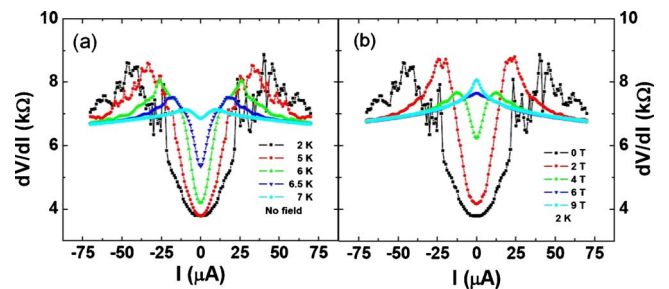

FIG. 7. (Color online) Current dependence of the differential resistance for sample 2 under (a) different temperatures and (b) different magnetic fields.

herence peaks at the boundaries of the gap are consistent with the critical current behavior of Josephson junction(s) at which voltage first appears (when the weak links are overcome).

In Fig. 6(b), we show the differential resistance variation as a function of measuring current at 2 K but under different perpendicular magnetic fields. The general behavior is seen to be similar to those in Fig. 6(a), in which the applied magnetic field may be viewed as having the effect of decreasing the transition temperature. The two plateaus and their associated gaps are clear indications of the progressive establishment of coherence in the system, in stages. The interesting curve here is the one for 2 T, at which the plateau resistance shifts from 1 kΩ for fields below that to the 2.3 kΩ plateau at or above it. This is in conjunction with a clear jump in the minimum resistance value (at $I=0$) between 2 and 3 T. Thus the 2 T field is obviously associated with the destruction of the weak links so that the two-probe and four-probe resistances diverge above that.

In contrast to sample 1, the differential resistance behavior of sample 2, shown in Figs. 7(a) and 7(b), displays only one resistance plateau at ~6.6 kΩ. This could be reasonable since the three-probe resistance is only a few hundred ohms, indicating few or no weak links. But perhaps the most striking difference lies in the existence of a differential resistance peak that is barely discernible in Fig. 7(a) but very prominent under a large magnetic field as seen in Fig. 7(b). We shall speculate on its nature in the next section. However, in spite of this difference it is clear from Fig. 7(a) that the quasigap disappears above 7.5 K. Thus, the appearance of the quasigap is to be associated with the resistive transition at 7.5 K. Also, from Fig. 7(b) it is also seen that there is a jump in the minimum differential resistance value between 2 and 4 T. We take the bottom of the differential resistance, 4.16 kΩ, to be the internal series resistance since it is approximately at this value [Fig. 7(a), the green curve] that the shape of the quasigap has changed from triangular to quadratic. This choice is also consistent with the BKT transition temperature behavior and its attendant $T_{BKT}=5.94$ K, seen below. Together with the three-probe results [inset in Fig. 2(b)], it is also clear from the $I=0$ value of the 2 K differential resistance curve in Fig. 7(a) that there is a ~4 kΩ contact resistance in sample 2 that is external to the system of nanotubes.

D. 1D superconducting behavior

It should be mentioned that in contrast to the behaviors presented above, we have also observed 1D superconducting $R(T)$ that is smoothly varying,[5] together with a differential resistance gap that is also smoothly varying. Both are qualitatively consistent with the predictions of the Langer-Ambegaokar-McCumber-Halperin theory,[15,16] in which the finite resistance is caused by thermally activated phase slips.[17] These data are insensitive to the magnetic field, expected for 1D systems with very small cross sections. Here the physical picture is that the thin, 1D superconducting wire acts as the critical link bridging the conducting paths between the two voltage electrodes. We shall present these results separately as they involve different underlying physics.

IV. PHYSICAL INTERPRETATION

We consider our nanotube arrays to comprise 1D superconducting elements each characterized by a complex Ginzburg-Landau[18] wave function ψ that is a function of the spatial variable x along the c axis. Starting at 15 K, the formation of superconducting condensate in the nanotubes is responsible for the magnetoresistance seen in the inset of Fig. 2(a). Owing to the one dimensionality of the nanotubes, strong long wavelength thermal fluctuations prevent the appearance of a sharp superconducting transition[2] in individual nanotubes. As the temperature is lowered, however, the superconducting condensate grows in magnitude and (as justified by the observed phenomena, which obviously involve coupled arrays of nanotubes) we expect the neighboring elements to be transversely coupled via a Josephson interaction energy $-J\cos(\varphi_i-\varphi_j)$, where φ_i denotes the phase of the wave function for the ith element, assumed to be a constant over the longitudinal coherence length along the c axis with J being proportional to the superconducting electron density $|\psi|^2$.

A. Charging energy considerations

As the Josephson coupling involves the transfer of charges, a natural consideration is the competing mechanism of the (Coulomb) charging effect, which is governed by two parameters, $\alpha_c=zJ/E_c$ (Ref. 19) and $\alpha_r=h/4e^2R_n$,[20,21] where the first parameter is the ratio of the Josephson coupling energy to the charging energy and the second parameter is related to the resistance parallel to the capacitance that is the source of the charging energy. Here, $z=6$ is the number of nearest neighbors, $E_c=(2e)^2/2\varepsilon C$ is the charging energy for a Cooper pair, $\varepsilon=6$ is the dielectric constant of the zeolite frame (essentially that of aluminum phosphate), R_n denotes the normal resistance (per square) in the ab plane, and C is the self-capacitance of a conducting nanotube surrounded by other conducting nanotubes. Whereas the charging energy tends to suppress superconductivity as it would require the charge carriers (implied by the Josephson coupling) to be energetically activated, the parallel resistance tends to favor superconductivity since the latter enhances electron delocalization. In the case of sample 1, $\alpha_r=h/4e^2R_n=1.25$ (for $R_n=5133$ Ω/□ as estimated below) and $\alpha_r=1.03$ for sample 2 ($R_n=6253$ Ω/□). For these values of α_r superconductivity is known to always exist at low enough temperatures. But for $\alpha_r=0$ (i.e., normal resistance=∞), the criterion for the existence of superconductivity is $\alpha_c\geq1$. Since C in this case is in the form of C_0L, where C_0 is a dimensionless constant and L is the length of the conducting nanotube; for $L\to\infty$ the charging energy is zero and therefore the condition $\alpha_c\geq1$ is always satisfied. Hence, the condition $\alpha_c=zJ/E_c>1$ may be translated into a requirement for the minimum length of the conducting nanotube segment in the limit of infinite (transverse) normal resistance. A finite element calculation yields $C_0=0.27$, implying $L\geq1.5$ μm if the normal resistance is infinite. However, the existence of a finite and fairly low normal resistance in our case, with $\alpha_r=1.25$ or 1.03, means a smaller lower bound for L.

B. Analogy with 2D spin system and the BKT transition

From the above considerations we conclude that the existence of Josephson coupling in the *ab* plane is at least not inconsistent with our experimental data. Since the Josephson coupling can be alternatively written as $-J(\vec{s}_i \cdot \vec{s}_j)$ where $\vec{s}$ denotes a unit vector in the transverse *ab* plane, there is thus an analogy to a 2D spin model in which it is well known that there can be vortex excitations, consisting of spins that form a closed loop. Moving vortices can destroy coherence in the transverse plane. However, vortices of opposite helicities interact as attractive 2D charges with a logarithmic potential. They can become bound pairs at a BKT transition temperature, below which one expects the establishment of transverse coherence in the *ab* plane. This in turn would quench the longitudinal fluctuations (since the transverse cross section becomes much larger and hence the energy barrier for phase slips increases dramatically), thereby establishing 3D superconducting regions separated by weak links.

It should be noted that besides the 2D spin systems in which a BKT transition was usually studied,[22,23] there have been extensive observations of BKT transition in superconducting thin films.[24,25] More recently, the appearance of BKT transition was also reported in bulk 3D high T_c superconductors.[26–29] Below we show that in spite of the fact that our system is not the standard 2D context in which the BKT transition was usually considered, experimental data nevertheless show surprisingly good agreement with its various predictions.

C. Manifestations consistent with the interpretation of a BKT transition

In support of our interpretation that the large resistance drop seen at 7.5 K is the result of a BKT transition in the transverse *ab* plane, we present evidences that show our $R(T)$ and nonlinear *I-V* characteristics to be consistent with the predictions of a BKT transition. A BKT transition is characterized by two temperatures: a T_{co} below which nonlinear *I-V* behavior is expected, and a $T_{BKT} < T_{co}$, which anchors the expected temperature dependence of resistance.

1. Nonlinear I-V characteristics

We can identify $T_{co} = 7.5$ K since below that temperature our differential resistance data clearly show the appearance of a triangular gap, implying $V \propto I^2$. The progressive variation from a constant R ($V \propto I$) at 7.5 K to a triangular quasi-gap ($V \propto I^2$) and then to a more rounded gap at below 6.5 K, is consistent with the BKT transition behavior of $V \propto I^\alpha$ with an α varying from 1 (at T_{co}) to 3 (at T_{BKT}) or larger with decreasing temperature.[24,30] From our differential resistance data $\alpha = 3$ (and hence T_{BKT}) should occurs at below 6.5 K but at or above ~6 K for both samples 1 and 2.

2. Temperature dependence of resistance

The resistance in the $I \to 0$ limit, measured relative to the internal series resistance, is predicted to vary with temperature as[31,32] $R - R_s = 10.8 b R_N \exp\{-2[b(T_{c0} - T_{BKT})/(T - T_{BKT})]^{1/2}\}$ for $T > T_{BKT}$. Here $R_s = 1.06$ kΩ is the lower pla-
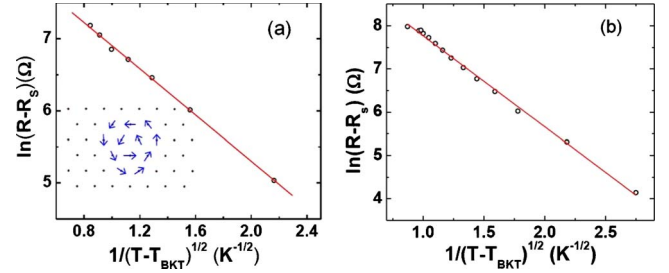

FIG. 8. (Color online) Theoretical fitting according to $\ell n(R - R_s) \propto (T - T_{BKT})^{-1/2}$ at $T > T_{BKT}$: (a) for sample 1 and (b) for sample 2. In (a), $T_{BKT} = 6.17$ K, and $R_s = 1.06$ kΩ is the lower plateau resistance value shown in Fig. 6. It arises from the weak links connecting the different superconducting regions. Inset: A schematic picture of the transverse plane perpendicular to the *c* axis, with each dot representing an end view of a segment of the 1D superconducting nanotube. A vortex excitation, indicated by arrows whose directions are given by the phase (angles) of the 1D wave function, is shown. In (b), $T_{BKT} = 5.94$ K, and $R_s = 4.16$ kΩ is the series resistance taken from the bottom of differential resistance at 6 K.

teau series resistance for sample 1, and $R_s = 4.16$ kΩ for sample 2. In Figs. 8(a) and 8(b), we show our data on samples 1 and 2 to be in excellent agreement with the above prediction. The parameter values obtained are $T_{BKT} = 6.17$ K and $b = 0.48$, with $R_N = 0.96$ kΩ for the normal sheet resistance in sample 1, and $T_{BKT} = 5.94$ K and $b = 0.71$, with $R_N = 2.55$ kΩ in sample 2.[33]

3. Consistency and interpretation of other manifestations

For the BKT transition, the specific heat peak is noted to occur at a temperature above T_{BKT}.[30,34–36] In our case the measured specific heat peak is at 11–12 K,[5] thus consistent with this prediction.

The effect of a magnetic field is mainly due to its influence on J through the suppression of superfluid/superconducting electron density, which has the effect of both shifting T_{BKT} to lower temperatures as well as diminishing the magnitude of the resistance drop associated with the transition.

Below 6 K, the development of a low resistance gap in the dV/dI vs I data in sample 1 is interpreted to be associated with the weak links turning superconducting, thereby leading to the formation of global coherence between the two voltage electrodes. In sample 2 this is also observed as the further lowering of the low-resistance gap at 6 K and below. The first turning point in the MR data, in the range of 2–3 T for both samples (perpendicular field), is associated with the destruction of weak links and hence the global coherence. That is also seen in sample 1 as the jump in the dV/dI plateau resistance value (from 1 to 2.3 kΩ) at this characteristic value of the magnetic field.

Figure 5 (for sample 2) shows that as the magnetic field increases beyond the first MR turning point, i.e., 2–3 T for the perpendicular field case and 5–6 T for the parallel field case, there is a continuous increase in resistance which is attributable to a decrease in the *ab* plane coherence, accom-
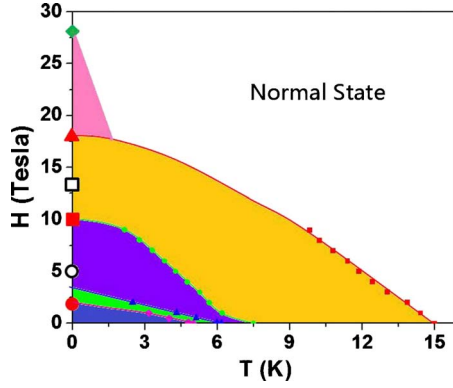
FIG. 9. (Color online) Magnetic field-temperature phase diagram summarized from the experiment data. Here yellow, violet, green, and blue regions denote, respectively, the fluctuating 1D superconducting regime, the nonlinear *I-V* regime, the regime in which the 3D superconducting regions are connected by weak links, and the global coherence regime. The solid symbols of circle, square and triangle on the vertical axis denote the demarcation points as measured by a perpendicular magnetic field at 50 mK. The open symbols are the corresponding points measured by a parallel field. The triangular region on the upper left denotes the FFLO state that is to be further verified.

panied by an increase in longitudinal fluctuations until at the second magnetoresistance turning point—10 T (perpendicular) and 13.5 T (parallel)—the system is basically reduced to being quasi-1D in character.

For a 1D superconductor orbital pair-breaking effects[37] are excluded due to the open nature of the Fermi surface. Then the Pauli paramagnetic limit for superconductivity eventually becomes of importance.[38,39] The disappearance of magnetic anisotropy at ~18 T may imply the suppression of superconducting condensate in individual nanotubes, i.e., the Pauli limit. Surprisingly, a finite slope persists up to 28 T as seen in the inset of Fig. 5. Therefore a natural question arises whether this slope still originates from superconducting correlations. Above the Pauli limiting field H_p, the Zeeman-split Fermi surfaces would no longer allow Cooper pairing with zero center-of-mass momentum. The theory of Fulde and Ferrell, as well as Larkin and Ovchinnikov (FFLO) (Ref. 40 and 41) predicts that type-II superconductors, when approaching H_p, have the possibility to increase their upper critical fields by "sacrificing" a part of their volume to the normal state. However, the Zeeman-split Fermi surfaces allow Cooper pairing only with a finite center-of-mass momentum. The superconductor may therefore create a spatial modulation of its order parameter, with wavelength on the order of the coherence length, and form the FFLO state in order to maintain superconductivity in fields beyond H_p. The finite slope may be a hint for the realization of such an FFLO state in this superconductor. This stimulates further high-magnetic field experiments in order to confirm this potential scenario. The overall behavior of our superconducting nanotube array may be summarized by a magnetic field-temperature phase diagram as shown in Fig. 9.

D. Magnetic field-temperature phase diagram

Since the overall characteristics of the two samples are rather similar, in Fig. 9 we use the perpendicular field data

for sample 1 to plot a magnetic field-temperature phase diagram. Here, yellow denotes the 1D fluctuating superconductor regime, the green line denotes T_{co} and the blue line denotes T_{BKT}, both associated with the BKT transition. Area colored by violet is the regime where one expects to see nonlinear *I-V* characteristics. Green is the regime in which the sample is characterized by inhomogeneous 3D superconducting regions connected by (normal) weak links. The bottom left corner is the regime of global coherence. Here, symbols are data, with the connecting solid line used to delineate the different regimes. The symbols on the vertical axis mark the positions of the first turning point, the second turning point and the merging point obtained from the 50 mK measurements. Here, the solid symbols are for the perpendicular case and the open symbols are for the parallel case. The triangular region on the upper left corner denotes the FFLO state as discussed above.

E. Estimates of physical parameters

Based on the physical interpretation presented above, we give some estimates of the relevant physical parameters.

1. Josephson coupling energy J

From $\pi J/k_B T_{BKT} \approx 1.12$ [Eq. (58) in Ref. 7] and T_{BKT} =6.2 K for sample 1 and T_{BKT}=5.94 K for sample 2, we obtain J=0.19 and 0.18 meV for samples 1 and 2, respectively.

2. Critical Josephson current I_c

From $I_c = 2eJ/\hbar$, we obtain $I_c \cong 0.092$ μA for sample 1 and $I_c \cong 0.088$ μA for sample 2.

3. Normal resistance R_n per square in the transverse plane

From $T_{BKT}/T_{co} = [1 + 0.173 R_n/(\hbar/e^2)]^{-1}$ [Eq. (9) in Ref. 23] and T_{BKT}=6.2 K, T_{co}=7.5 K for sample 1 and T_{BKT} =5.94 K, T_{co}=7.5 K for sample 2, we obtain R_n =5133 $\Omega/\square$ for sample 1. This value has been used in calculating the value of α_r=1.2 in Fig. 4(a). For sample 2, we have R_n=6253 $\Omega/\square$. These values of R_n should be compared with those of R_N obtained from fitting the temperature dependence in Fig. 8. Differences between the two are interpreted as being due to the (nonsquare) aspect ratio of the superconducting regions in the *ab* plane.

4. Superconducting gap parameter Δ at the transition temperature

From $I_c = (\pi\Delta(T_{BKT})/2eR_n)\tanh[\Delta(T_{BKT})/2k_B T_{BKT}]$ (Ref. 42) we obtain $\Delta(T_{BKT}=6.2$ K$) \approx 0.6$ meV for sample 1 and $\Delta(T_{BKT}=5.9$ K$) \approx 0.63$ meV for sample 2.

5. Coherence lengths

If we interpret that for the BKT transition, the perpendicular $H_{c2\perp} \approx 10$ T$/\mu_0$, and $H_{c2\parallel} \approx 13.5$ T$/\mu_0$ for the parallel field (both measured at 50 mK), then from these values we can obtain a transverse coherence length $\xi_{ab}(0)$ $=(\phi_0/2\pi\mu_0 H_{c2\parallel})^{1/2} \approx 5.0$ nm and a longitudinal coherence length (along the *c* axis) $\xi_{c-axis}(0)=\phi_0/[2\pi\mu_0 H_{c2\perp}\xi_{ab}(0)]$

≈ 6.6 nm. Here $\phi_0 = hc/2e$ is the quantum flux. These two values are surprisingly close. A possible interpretation is that the coherence length along the c axis is modulated by fluctuation effects.

6. Number of participating nanotubes

We first focus on sample 1. In Fig. 6(a), there are two critical currents. The smaller one with the value of 16.8 μA (black curve, 2 K) is the Josephson critical current responsible for overcoming the weak links along the c axis. The larger one with the value of 36.0 μA (blue curve, 6 K) may be regarded as the critical current for the BKT transition.

From $I_0 = 36$ μA $= w e k_B T_{\text{BKT}}/\hbar \xi_c$ [Eq. (36b) in Ref. 31], we have $I_0 = 36$ μA $= w/\xi_c \times 0.129$ μA where w/ξ_c gives the effective number of participating Josephson junctions contacted by the surface electrode. Since 0.129 μA is roughly the critical current I_c estimated above (both are on the order of 0.1 μA), we take $\xi_c = 1.37$ nm to be the unit cell length, implying $w \approx 382$ nm along the transverse plane that is parallel to the sample-surface electrode interface. Along the depth direction (in the transverse ab plane but perpendicular to the surface electrode), we note that from the fit to the measured temperature variation of the resistance we have $R_N = 980$ $\Omega/2 = 490$ Ω (the factor of 2 comes from the consideration of the return path to the surface electrode). Since $R_n = 5133$ $\Omega/\square$ as estimated above, a comparison between the two values implies an effective aspect ratio of ~10.5 between the width and depth. Therefore the effective sample size in the depth direction is ~36 nm. Taken together, we estimate that there are ~7460 nanotubes participating in the observed superconducting transition.

For sample 2, from the estimated parameter values $I_0 = 25.7$ μA $= w/\xi_c \times 0.124$ μA, we obtain $w \approx 284$ nm so that the effective aspect ratio of 5 leads to a depth estimate of 57 nm. Hence there are about 8750 participating nanotubes in sample 2.

F. Speculation on the origin of the differential resistance peak

The differential resistance peak seen in Fig. 7(b) is a clear indication that there is a mechanism operating in our system that competes with superconductivity. We speculate on three possible origins: Peierls transition, Luttinger liquid, and granular contact(s). The first two may lead to a quasigap in the nanotube density of states that is manifest as a peak in resistance. Both are associated with 1D microgeometry and may be significantly suppressed when the nanotubes are transversely coupled. The fact that the peak and the resistance gap can coexist over certain magnetic field and temperature ranges may imply that the superconductivity and the competing effect exist on geometrically separate parts of the sample, and what was observed is the overall resistance of a complex, inhomogeneous network. Such an interpretation is attractive because then the effect of the magnetic field is to first break the weakest parts of the Josephson-coupled network so that some parts may exhibit the quasi-1D behavior. The differences in the transverse coupling may arise due to the amount of overlap (of the superconducting segments along the c-axis direction) between the neighboring nanotubes. Thus, a significant amount of overlap throughout the participating nanotubes in the sample can lead to a smaller normal state resistance per square in the ab plane, as well as the absence of a resistance peak. This could be the difference between sample 1 and sample 2.

Granular metallic contacts can also cause resistance peaks, but the magnetic field dependence is more difficult to explain. However, such a mechanism cannot be completely ruled out at present.

V. CONCLUDING REMARKS

Together with previous evidences,[4,5] the fact that carbon nanotubes can be superconducting is now beyond reasonable doubt. As the measured results are repeatable and consistent, the likelihood that the superconductivity is the result of unintentional doping, is also greatly diminished. The role of the AFI zeolite matrix, beyond the physical regulation of the nanotube separation, has been examined through density functional theory calculations[43] and shown to be relatively minor in the electronic sense. Hence, it may be concluded that the nanostructuring of carbon in the form of tubes can indeed lead to superconductivity as predicted.[1] The similarity of our data with the behaviors exhibited by the known 1D superconductors $Tl_2Mo_6Se_6$ (Ref. 44) is a further support to this conclusion. In this context it should be noted that some earlier data obtained on ropes of nanotubes[45–48] also exhibit some similarity to ours, although the physical interpretation of how it comes about is qualitatively different.[49]

Our experience has shown that the use of close electrode separation, together with the consequent small room temperature sample resistance, is a necessity to observe superconductivity. That implies impurities and defects present in most nanotube samples could be responsible for masking some of the intrinsic nanotube characteristics at the scale of 0.5 μm or above. This is reasonable as impurities and defects are much more effective in localizing electrons in 1D than they are in higher dimensions.

This work also opens up many intriguing problems/ phenomena not yet completely understood. For example, the large coherence peaks seen in the 2 T curve of Fig. 6(b) still remain unexplained, so too is the nature of the resistance peak seen in Fig. 7(b). However, the most fundamental question is the nature of the electron-electron coupling that leads to the observed superconductivity. Thus, the isotope effect, the removal of the AFI matrix, the continued improvement of sample quality, etc, are the tasks to be actively pursued.

*Present address: Research and Development, King Abdullah University of Science and Technology, Thuwal, Saudi Arabia.

†Corresponding author; sheng@ust.hk

[1] L. X. Benedict, V. H. Crespi, S. G. Louie, and M. L. Cohen, Phys. Rev. B **52**, 14935 (1995).

[2] D. Mermin and H. Wagner, Phys. Rev. Lett. **17**, 1133 (1966); P. C. Hohenberg, Phys. Rev. **158**, 383 (1967).

[3] R. E. Peierls, *Quantum Theory of Solids* (Oxford University, Oxford, 1955).

[4] Z. K. Tang, L. Z. Zhang, N. Wang, X. X. Zhang, G. H. Wen, G. D. Li, J. N. Wang, C. T. Chan, and P. Sheng, Science **292**, 2462 (2001).

[5] R. Lortz, Q. C. Zhang, W. Shi, J. T. Ye, C. Y. Qiu, Z. Wang, H. T. He, P. Sheng, T. Z. Qian, Z. K. Tang, N. Wang, X. X. Zhang, J. N. Wang, and C. T. Chan, Proc. Natl. Acad. Sci. U.S.A. **106**, 7299 (2009).

[6] V. L. Berezinskii, Sov. Phys. JETP **32**, 493 (1971); **34**, 610 (1972).

[7] J. M. Kosterlitz and D. J. Thouless, J. Phys. C **6**, 1181 (1973).

[8] W. M. Meier and D. H. Olson, Zeolites **12**, 1 (1992).

[9] N. Wang, Z. K. Tang, G. D. Li, and J. S. Chen, Nature (London) **408**, 50 (2000).

[10] H. D. Sun, Z. K. Tang, J. Chen, and G. Li, Solid State Commun. **109**, 365 (1999).

[11] I. L. Li, G. D. Li, H. J. Liu, C. T. Chan, and Z. K. Tang, Appl. Phys. Lett. **82**, 1467 (2003).

[12] Z. M. Li, Z. K. Tang, H. J. Liu, N. Wang, C. T. Chan, R. Saito, S. Okada, G. D. Li, J. S. Chen, N. Nagasawa, and S. Tsuda, Phys. Rev. Lett. **87**, 127401 (2001).

[13] H. J. Liu and C. T. Chan, Phys. Rev. B **66**, 115416 (2002).

[14] Both samples shown here differ from the one whose electrical resistance vs temperature was shown in Ref. 5, which reflects the behavior of a 1D (fluctuating) superconducting bundle that presumably acts as the critical link bridging the conducting path.

[15] J. S. Langer and V. Ambegaokar, Phys. Rev. **164**, 498 (1967).

[16] D. E. McCumber and B. I. Halperin, Phys. Rev. B **1**, 1054 (1970).

[17] T. Z. Qian, W. Q. Ren, and P. Sheng, Phys. Rev. B **72**, 014512 (2005).

[18] M. Tinkham, *Introduction to Superconductivity*, 2nd ed. (MGH, New York, 1996), Chap. 4.

[19] F. P. Mancini, P. Sodano, and A. Trombettoni, Phys. Rev. B **67**, 014518 (2003).

[20] S. Chakravarty, S. Kivelson, G. T. Zimanyi, and B. I. Halperin, Phys. Rev. B **35**, 7256 (1987).

[21] A. Kampf and G. Schon, Phys. Rev. B **36**, 3651 (1987).

[22] S. Doniach and B. A. Huberman, Phys. Rev. Lett. **42**, 1169 (1979).

[23] M. R. Beasley, J. E. Mooij, and T. P. Orlando, Phys. Rev. Lett. **42**, 1165 (1979).

[24] A. F. Hebard and A. T. Fiory, Phys. Rev. Lett. **44**, 291 (1980); **50**, 1603 (1983).

[25] D. J. Resnick, J. C. Garland, J. T. Boyd, S. Shoemaker, and R. S. Newrock, Phys. Rev. Lett. **47**, 1542 (1981).

[26] S. Martin, A. T. Fiory, R. M. Fleming, G. P. Espinosa, and A. S. Cooper, Phys. Rev. Lett. **62**, 677 (1989).

[27] A. K. Pradhan, S. J. Hazell, J. W. Hodby, C. Chen, Y. Hu, and B. M. Wanklyn, Phys. Rev. B **47**, 11374 (1993).

[28] R. Sugano, T. Onogi, and Y. Murayama, Phys. Rev. B **48**, 13784 (1993).

[29] B. Chattopadhyay and S. R. Shenoy, Phys. Rev. Lett. **72**, 400 (1994).

[30] H. Q. Ding and M. S. Makivic, Phys. Rev. B **42**, 6827 (1990).

[31] B. I. Halperin and D. R. Nelson, J. Low Temp. Phys. **36**, 599 (1979).

[32] D. W. Abraham, C. J. Lobb, M. Tinkham, and T. M. Klapwijk, Phys. Rev. B **26**, 5268 (1982).

[33] As the occupation fraction for the superconducting nanotubes in the transverse plane must be less than 100%, it remains an open possibility that the transition temperature could be dependent on the fraction of superconducting nanotubes in the zeolite pores (Refs. 50 and 51).

[34] R. Gupta and C. F. Baillie, Phys. Rev. B **45**, 2883 (1992).

[35] R. Gupta, J. DeLapp, G. G. Batrouni, G. C. Fox, C. F. Baillie, and J. Apostolakis, Phys. Rev. Lett. **61**, 1996 (1988).

[36] J. Tobochnik and G. V. Chester, Phys. Rev. B **20**, 3761 (1979).

[37] L. P. Gorkov, Sov. Phys. JETP **10**, 593 (1960).

[38] A. K. Clogston, Phys. Rev. Lett. **9**, 266 (1962).

[39] B. S. Chandrasekhar, Appl. Phys. Lett. **1**, 7 (1962).

[40] P. Fulde and R. A. Ferrell, Phys. Rev. **135**, A550 (1964).

[41] A. I. Larkin and Y. N. Ovchinnikov, Sov. Phys. JETP **20**, 762 (1965).

[42] V. Ambegaokar and A. Baratoff, Phys. Rev. Lett. **10**, 486 (1963); **11**, 104(E) (1963).

[43] H. J. Liu, Z. M. Li, Q. Liang, Z. K. Tang, and C. T. Chan, Appl. Phys. Lett. **84**, 2649 (2004).

[44] B. Bergk, R. Lortz, A. Petrovic, Z. Wang, D. Salloum, P. Gougeon, and M. Potel (unpublished).

[45] M. Kociak, A. Yu. Kasumov, S. Gueron, B. Reulet, I. I. Khodos, Yu. B. Gorbatov, V. T. Volkov, L. Vaccarini, and H. Bouchiat, Phys. Rev. Lett. **86**, 2416 (2001).

[46] A. Kasumov, M. Kociak, M. Ferrier, R. Deblock, S. Gueron, B. Reulet, I. Khodos, O. Stephan, and H. Bouchiat, Phys. Rev. B **68**, 214521 (2003).

[47] A. De Martino and R. Egger, Phys. Rev. B **70**, 014508 (2004).

[48] M. Ferrier, A. De Martino, A. Kasumov, S. Gueron, M. Kociak, R. Egger, and H. Bouchiat, Solid State Commun. **131**, 615 (2004).

[49] In Refs. 40–43, the mentioned BKT transition refers to the binding-unbinding transition of quantum phase slips of opposite helicities so that a zero-resistance state becomes possible even in a 1D superconducting wire. This is in contrast to the BKT transition in the transverse plane that mediates a 1D to 3D crossover.

[50] X. C. Zeng, D. Stroud, and J. S. Chung, Phys. Rev. B **43**, 3042 (1991).

[51] Y. J. Yun, I.-C. Baek, and M. Y. Choi, Phys. Rev. Lett. **97**, 215701 (2006).